学位論文
Doctoral Thesis

Effect of iodine concentration and body size on iodine subtraction in virtual non-contrast imaging: A phantom study
（仮想非造影画像におけるヨードサブトラクションに対するヨード濃度と体格の影響：ファントム研究）

白坂　崇

Takashi Shirasaka

指導教員

船間　芳憲　教授
熊本大学大学院保健学教育部博士後期課程保健学専攻

2024年3月

甲　中表紙

学位論文
Doctoral Thesis

論文題名　：　Effect of iodine concentration and body size on iodine subtraction invirtual non-contrast imaging: A phantom study
（仮想非造影画像におけるヨードサブトラクションに対するヨード濃度と体格の影響：ファントム研究）

著 者 名　：　白坂 崇
Takashi Shirasaka

指導教員名　：　熊本大学大学院保健学教育部博士後期課程保健学専攻　船間　芳憲　教授

審査委員名　：　主 査　　教 授　　藤原 康博
副 査　　教 授　　北島 美香
副 査　　教 授　　船間 芳憲

2024年3月

Radiography 29 (2023) 557–563

Contents lists available at ScienceDirect

Radiography

journal homepage: www.elsevier.com/locate/radi

Effect of iodine concentration and body size on iodine subtraction in virtual non-contrast imaging: A phantom study

T. Shirasaka [a, b, *], T. Kojima [b, c], S. Yamane [b], R. Mikayama [b], M. Kawakubo [d], R. Funatsu [b], T. Kato [b], K. Ishigami [e], Y. Funama [f]

[a] Graduate School of Health Sciences, Kumamoto University, 4-24-1 Kuhonji, Kumamoto, 862-0976, Japan
[b] Division of Radiology, Department of Medical Technology, Kyushu University Hospital, 3-1-1 Maidashi, Higashi Ward, Fukuoka, 812-8582, Japan
[c] Department of Health Sciences, Graduate School of Medical Sciences, Kyushu University, 3-1-1 Maidashi, Higashi Ward, Fukuoka, 812-8582, Japan
[d] Department of Health Sciences, Faculty of Medical Sciences, Kyushu University, 3-1-1 Maidashi, Higashi Ward, Fukuoka, 812-8582, Japan
[e] Department of Clinical Radiology, Graduate School of Medical Sciences, Kyushu University, 3-1-1 Maidashi, Higashi Ward, Fukuoka, 812-8582, Japan
[f] Department of Medical Radiation Sciences, Faculty of Life Sciences, Kumamoto University, 4-24-1 Kuhonji, Kumamoto, 862-0976, Japan

ARTICLE INFO

Article history:
Received 23 October 2022
Received in revised form
19 February 2023
Accepted 5 March 2023

Keywords:
Dual-energy computed tomography
Virtual non-contrast
Iodine subtraction
Iodine concentration
Body size

ABSTRACT

Introduction: Dual-energy computed tomography (DECT) can generate virtual non-contrast (VNC) images. Herein, we sought to improve the accuracy of VNC images by identifying the optimal *slope of contrast media* (SCM) for VNC-image generation based on the iodine concentration and subject's body size.

Methods: We used DECT to scan a multi-energy phantom including four iodine concentration rods (15, 10, 5, and 2 mg/mL), and 240 VNC images (eight SCM ranging from 0.49 to 0.56 × three body sizes × ten scans) that were generated by three-material decomposition. The CT number of each iodine and solid water rod part was measured in each VNC image. The difference in the CT number between the iodine and the solid water rod part was calculated and compared using paired *t*-test or repeated measures ANOVA.

Results: The SCM that achieved an absolute value of the difference in CT number of <5.0 Hounsfield units (HU) for all body sizes simultaneously was greater at lower iodine concentration (SCM of 0.5, 0.51, and 0.53 at 10, 5, and 2 mg/mL iodine, respectively). At an iodine concentration of 15 mg/mL, no SCM achieved an absolute difference of <5.0 HU in CT number for all body sizes simultaneously. At all iodine concentrations, the SCM achieving the minimal difference in the CT number increased with the increase in body size.

Conclusion: By adjusting the SCM according to the iodine concentration and body size, it is possible to generate VNC images with an accuracy of <5.0 HU.

Implications for practice: Improving the accuracy of VNC images minimizing incomplete iodine subtraction would make it possible to replace true non-contrast (TNC) images with VNC images and reduce the radiation dose.

Introduction

Dual-energy computed tomography (DECT) is a promising imaging technique that provides better abdominal tissue characterization compared to single-energy computed tomography.[1–3] DECT allows for the generation of virtual non-contrast (VNC) images by visually subtracting the iodine signal from contrast-enhanced images. Several research groups have reported that in tri-phasic abdominal CT imaging, replacing true non-contrast (TNC) images with VNC images obtained from contrast-enhanced DECT can reduce the radiation dose by 25%–35%.[4–10] However, despite the

* Corresponding author. Graduate School of Health Sciences, Kumamoto University, 4-24-1 Kuhonji, Kumamoto, 862-0976, Japan.
E-mail addresses: shirasaka.takashi.154@m.kyushu-u.ac.jp (T. Shirasaka), kojima.tsukasa.929@m.kyushu-u.ac.jp (T. Kojima), yamane.shiho.439@m.kyushu-u.ac.jp (S. Yamane), mikayama.ryoji.923@m.kyushu-u.ac.jp (R. Mikayama), kawakubo.masateru.968@m.kyushu-u.ac.jp (M. Kawakubo), funatsu.ryohei.132@m.kyushu-u.ac.jp (R. Funatsu), kato.toyoyuki.715@m.kyushu-u.ac.jp (T. Kato), ishigami.kosei.581@m.kyushu-u.ac.jp (K. Ishigami), funama@kumamoto-u.ac.jp (Y. Funama).

https://doi.org/10.1016/j.radi.2023.03.003
1078-8174/

reported usefulness of VNC images in terms of the patient radiation dose, the complete replacement of TNC with VNC in terms of image quality remains controversial, especially due to the risk of incomplete iodine subtraction.[3,6,8,11–15] In other words, improving the accuracy of iodine subtraction is essential in order to reduce the radiation dose by replacing TNC with VNC.

In DECT, two different energies provide different contrasts depending on the composition of each tissue, making it possible to generate images that isolate specific tissue components. One of the methods used in DECT is the three-material-decomposition algorithm. The input parameters used for the three-material-decomposition algorithm are the CT numbers for fat and for soft tissue for high- and low-keV images, plus the *slope of contrast media* (SCM) value. The SCM represents the percentage change in the iodinated CT number between low- and high-keV virtual monochromatic images. The SCM is the most important parameter for the generation of VNC images by the three-material-decomposition algorithm. If an inappropriate SCM value is used, incomplete iodine subtraction images may be obtained. Borhani et al. pointed out that further optimization of the material decomposition algorithm by the vendor is needed to bring the CT number in VNC closer to the CT number based on TNC acquisition.[15] Factors that can cause incomplete iodine subtraction include the scan phase used to generate the VNC[6,7,9] and the subject's body size.[10,16] We therefore speculated that it would be important to optimize the SCM in terms of the iodine concentration and subject's body size to obtain accurate VNC images. We conducted the present study to identify the optimal SCM value for generating VNC images based on the iodine concentration, and to determine the trend of the change in optimal SCM value according to the subject's body size.

Methods

This was an experimental phantom study, with no requirement for institutional review board approval.

Endpoints

The primary endpoints of the study were to identify the feasible SCM value at which the difference in the CT number between the iodine-subtracted part and the background in VNC images was <5 Hounsfield units (HU), and to determine the trend of the change in optimal SCM value depending on the iodine concentration and subject's body size.

Phantoms

A multi-energy phantom system (Model 1472; Gammex RMI, Middleton, WI, USA) was used; it contains cylindrical holes for the placement of various rods of the reference materials. Four iodine concentration rods (15, 10, 5, and 2 mg/mL) were placed evenly throughout the phantom. Adipose, blood, and brain rods were used for the purpose of filling all remaining holes in the rod insertion area. We used rods other than iodine with as low an attenuation value as possible to minimize artifacts. The manufacturer's specifications of nine rods representing different materials were as follows. #1: adipose ($\rho_e w = 0.94$); #2: iodine (2 mg/mL); #3: blood ($\rho_e w = 1.03$); #4: iodine (15 mg/mL); #5: brain ($\rho_e w = 1.02$); #6: iodine (10 mg/mL); #7: blood ($\rho_e w = 1.07$); #8: iodine (5 mg/mL); #9: solid water ($\rho_e w = 1.00$). The $\rho_e w$ indicates a relative value of 3.3439×1023 m^{-3} for the electron density of water. For the representation of various body sizes, a multi-energy phantom with and one without an attached oval annulus was used (CTP579-10 and CTP651-10; The Phantom Laboratory, Salem, NY).

Fig. 1 shows the small, medium, and large body sizes of the multi-energy phantom (small body size: circular water-equivalent 20-cm diameter section; medium body size: small body size with an attached oval annulus 25-cm high × 35-cm wide with a 95-cm circumference; large body size: small body size with an attached oval annulus 30-cm high × 38-cm wide with a 107-cm circumference). The water-equivalent elliptical areas of these phantoms displayed on the CT system were 335, 655.9, and 860.2 cm^2, respectively.

Image acquisition and reconstruction

The phantom was scanned by a single-source DECT scanner with rapid kilovolt-switching and deep learning spectral reconstruction (Aquilion One PRISM Edition; Canon Medical Systems, Otawara, Japan). In accordance with the typical clinical scanning protocol, all DECT images were acquired using helical scanning. A fixed radiation dose (CT dose index volume of 17.8 mGy) was used to suppress the effect of dose dependence.[17] To compensate for directional dependency, ten scans were performed so that the starting position of each x-ray irradiation was shifted by 36° (ten consecutive scans were performed with the scan start time interval of each scan shifted by 10% of the rotation time).[18]

The scanning parameters were as follows. Tube voltages of the dual-energy scanning: 135 and 80 kVp; tube current: 650 mA; rotation time: 0.5 s; collimation: 80 × 0.5 mm; pitch: 0.813. All

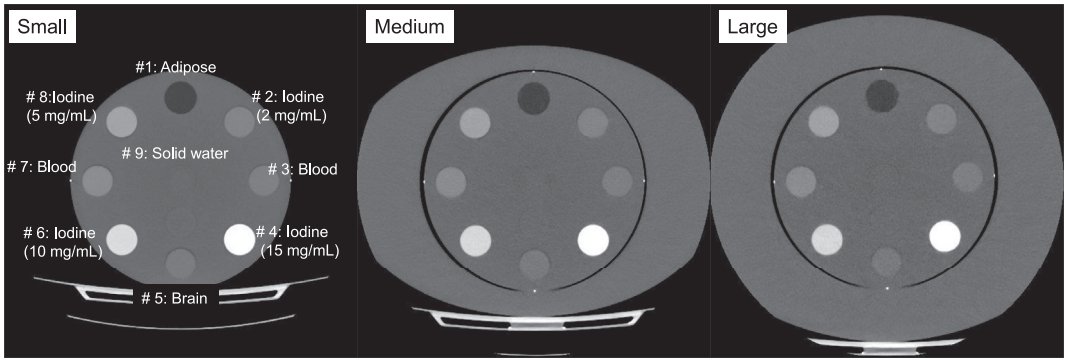

Figure 1. Axial image of the multi-energy phantom. Four iodine concentration rods with iodine concentrations at 15, 10, 5, and 2 mg/mL were located at #4, #6, #8, and #2, respectively. For assuming small, medium, and large body sizes, the multi-energy phantom was attached with and without an oval annulus. The water-equivalent elliptical area of each phantom displayed on the CT system was 335, 655.9, and 860.2 cm^2, respectively. The rod numbers were as follows. #1: Adipose ($\rho_e w = 0.94$). #2: Iodine (2 mg/mL). #3: Blood ($\rho_e w = 1.03$). #4: Iodine (15 mg/mL). #5: Brain ($\rho_e w = 1.02$). #6: Iodine (10 mg/mL). #7: Blood ($\rho_e w = 1.07$). #8: Iodine (5 mg/mL). #9: Solid water ($\rho_e w = 1.00$).

images were reconstructed with a slice thickness of 0.5 mm using the spectral reconstruction parameter of a body standard.

CT image post-processing and image analysis

With the DE scanning using our CT system, two basis material images (a water and an iodine image) were first reconstructed for the DE analysis. The VNC image was then generated from the virtual monochromatic images at 60 keV as the low keV and at 80 keV as the high keV. The resulting VNC image was an image with iodine subtraction based on the 80-keV image.

Determination of the CT-number ratio using 60-keV and 80-keV images

Thirty 60-keV and 80-keV images (three body sizes × ten scans) at 5.0 mm thickness were generated by a three-material-decomposition algorithm at a commercially available workstation (Vitrea; Canon Medical Systems, Otawara, Japan). We determined the CT number in each iodine rod part by using a region of interest (ROI) of 20 mm diameter. We calculated the ratio of the CT number for the 80 keV to that for the 60 keV for each iodine concentration.[19]

Determining the optimal input value of SCM for VNC

The 5.0-mm-thick VNC images were generated using vendor-recommended standard settings. The settings were as follows. *Material 1*, CT numbers for fat: −122 and −97 HU at 60 and 80 keV, respectively; *Material 2*, CT numbers for soft tissue: 60 and 61 HU at 60 and 80 keV, respectively; SCM: 0.51. We generated 240 VNC images (eight SCM × three body sizes × ten scans) by varying the SCM value from 0.49 to 0.56 with an interval of 0.01. The CT number of each iodine rod and solid water rod part in the VNC image was measured using a 20 mm diameter ROI. We calculated the difference in the CT number between the iodine rod and the solid water rod part. We identified feasible SCM values that achieved a mean difference in CT number of less than 5 HU and a 95% confidence interval (95% CI) of less than 5 HU for each body size. The optimal input value of SCM was defined as the value that achieves a minimum difference in the CT number among feasible SCM values.

Statistical analysis

For the ratio of the CT number for the 80 keV to that for the 60 keV images, summary statistics were generated using the mean and standard deviation. Summary statistics were constructed with the use of means with 95% CIs for the other continuous variables. As a post hoc analysis, repeated measures ANOVA with Bonferroni post-hoc correction (for multiple comparisons) was used to compare the CT numbers of the optimal SCM value and the other feasible SCM values. For comparisons between two data points (one optimal and one feasible SCM value), a paired t-test was applied. The statistical significance level was set at 0.05. Statistical software (R Package ver. 4.1.0; R Foundation for Statistical Computing, Vienna, Austria) was used for the statistical analysis.[20]

Results

Table 1 provides the ratio of the CT number for the 80 keV to the CT number for the 60 keV images at each iodine concentration and body size. At the higher iodine concentrations (15 and 10 mg/mL), the ratios of the CT number were similar among the three body sizes. At the 2 mg/mL iodine concentration, the ratio of the CT number became slightly smaller with the increase in body size.

Table 1
Ratio of the CT number for the 80 keV to that for the 60 keV images.

Body size	Iodine concentration			
	15 mg/mL	10 mg/mL	5 mg/mL	2 mg/mL
Small	0.523 ± 0.0015	0.508 ± 0.0020	0.529 ± 0.0014	0.584 ± 0.0032
Medium	0.524 ± 0.0013	0.507 ± 0.0030	0.519 ± 0.0041	0.574 ± 0.0073
Large	0.524 ± 0.0017	0.506 ± 0.0037	0.521 ± 0.0089	0.570 ± 0.0130

Data are shown as mean value ± standard deviation.

Fig. 2 shows the generated axial VNC images with varying SCM values under the condition of a small, medium, and large body size.

Tables 2–5 show the changes in the absolute differences in the CT numbers between the iodine concentration and water in the VNC images. At the iodine concentration of 15 mg/mL, except when the SCM value of 0.52 was used for the medium body size, differences in the CT number of <5 HU could not be achieved (Table 2). At the 10 mg/mL iodine concentration, the optimal SCM value was 0.5 for all body sizes (Table 3). At the iodine concentration of 5 mg/mL, the optimal SCM values were 0.50, 0.51, and 0.51 for the small, medium, and large body size, respectively. Significant difference was observed between the optimal and the other feasible SCM value at the small body size (Table 4). At the 2 mg/mL iodine concentration, four feasible SCM values were observed in the small body size. Among them, the optimal SCM value was 0.52. At the medium body size, the optimal SCM value was 0.53. Significant difference was not observed between the SCM values of 0.53 and 0.54 ($p = 0.999$), or between the SCM values of 0.53 and 0.55 ($p = 0.334$). For large body size, the SCM value of 0.55 was the optimal value. There was no significant difference among the optimal and feasible SCM values.

The line charts in Fig. 3a–d shows the changes in the absolute differences in the CT numbers between the iodine concentration and water in the VNC images, cropped near the SCM value where the difference in the CT number is the smallest, at different body sizes. For all iodine concentrations, the SCM value that achieved the smallest absolute difference in CT number with 95% CIs of <5 HU increased as the body size increased. The SCM value that achieved the absolute value of the difference in CT number with 95% CIs of <5 HU for all body sizes simultaneously was greater with a lower iodine concentration (10, 5, and 2 mg/mL: 0.5, 0.51, and 0.53 of the SCM value, respectively).

Fig. 4a–d depicts the mean CT number in VNC images for each iodine concentration and body size combination when varying the SCM value. At all iodine concentrations, the SCM value at which the CT number approached zero increased with the increase in body size. The difference in the CT number due to the change in the SCM value was greater for the higher iodine concentrations.

The line charts in Fig. 5 illustrate the mean CT number of the solid water rod for each body size in VNC images under various SCM values. The CT number in the solid water decreased with the increase in the SCM value. The smaller the body size was, the larger the magnitude of the change in CT number was with the increase in SCM.

Discussion

These experiments demonstrated that the optimal *slope of contrast media* (SCM) value for generating VNC images by the three-material decomposition algorithm varied depending on the iodine concentration and subject's body size. The accuracy of VNC can be improved by changing the SCM value depending on the scan phase during which the iodine subtraction is performed (i.e., the iodine concentration). Although the change in the SCM value according to

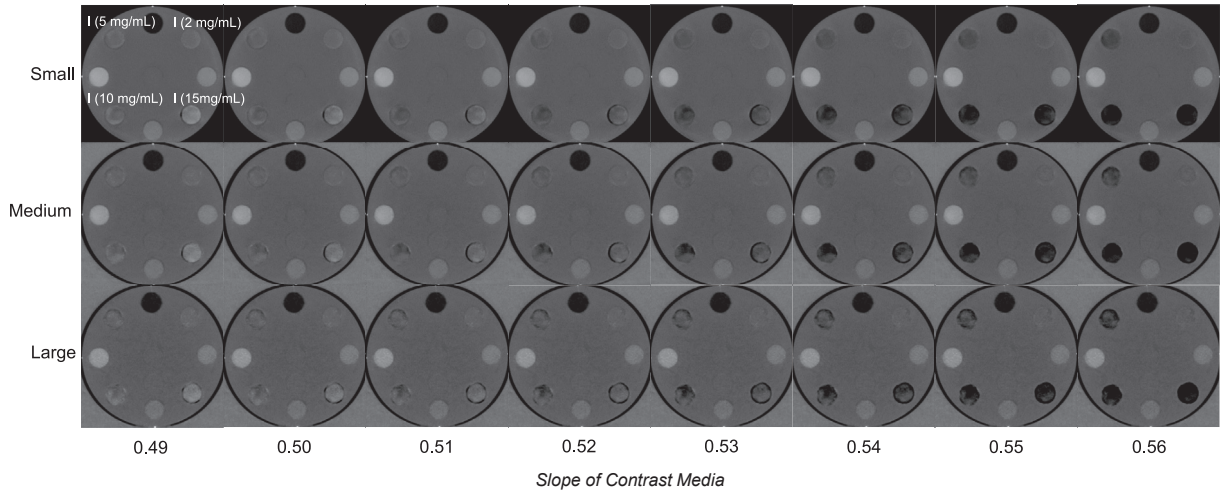

Figure 2. The clipped axial VNC images with varying *Slope of Contrast Media* (SCM) values under the assumption of small, medium, and large body sizes. The SCM was varied from 0.49 to 0.56. The rod numbers are explained in the legend of Fig. 1.

Table 2
Difference in the CT number between the iodine-subtracted part and the background at 15 mg/mL iodine concentration.

Body size	*Slope of contrast media* value							
	0.49	0.50	0.51	0.52	0.53	0.54	0.55	0.56
Small	31.3 (30.0–32.6)	18.5 (17.2–19.8)	5.3 (4.0–6.7)	7.3 (6.1–8.5)	19.3 (18.0–20.6)	36.6 (34.8–38.3)	56.8 (55.1–58.6)	75.9 (74.3–77.5)
Medium	34.7 (33.4–36.1)	23.0 (21.8–24.2)	11.8 (10.6–12.9)	**1.6 (0.9–2.3)**	10.7 (9.3–2.08)	27.7 (25.7–29.8)	49.3 (47.2–51.4)	69.6 (67.8–71.5)
Large	36.4 (34.8–37.9)	25.4 (23.9–26.9)	14.9 (13.5–16.4)	4.4 (2.9–5.8)	7.8 (6.1–9.6)	24.5 (22.2–26.7)	45.3 (42.6–47.9)	66.8 (64.4–69.2)

Data are shown as mean value (Hounsfield units) and 95% confidence interval (lower–upper). Numbers in bold are the values at the optimal *slope of contrast media* (SCM) value for each body size. The feasible SCM values were not obtained for the small and large body sizes. For the medium body size, only one feasible SCM value (the slope of contrast media at 0.52) was obtained, and it was defined as optimal. Therefore, no statistical analysis was performed in each body size.

Table 3
Difference in the CT number between the iodine-subtracted part and the background at 10 mg/mL iodine concentration.

Body size	*Slope of contrast media* value							
	0.49	0.50	0.51	0.52	0.53	0.54	0.55	0.56
Small	5.4 (4.4–6.4)	**3.2 (2.1–4.2)**	11.3 (10.4–12.3)	19.8 (18.7–21.0)	30.2 (28.9–31.5)	43.3 (42.0–44.6)	57.4 (56.1–58.8)	71.1 (69.8–72.4)
Medium	7.8 (6.2–9.4)	**1.8 (0.9–2.7)**	7.0 (5.3–8.8)	15.9 (13.7–18.0)	26.9 (24.4–29.4)	39.9 (37.0–42.8)	54.3 (51.3–57.3)	68.9 (66.1–71.7)
Large	10.0 (8.4–11.7)	**3.4 (2.0–4.8)**	4.1 (2.2–5.9)	13.0 (10.7–15.2)	24.4 (21.5–27.3)	38.0 (34.7–41.3)	52.7 (49.4–55.9)	67.5 (64.5–70.4)

Data are shown as mean value (Hounsfield units) and 95% confidence interval (lower–upper). Numbers in bold are the values at the optimal *slope of contrast media* value for each body size. Only optimal *slope of contrast media* value (slope of contrast media at 0.50) was obtained in each body size. Therefore, no statistical analysis was performed in each body size.

Table 4
Difference in the CT number between the iodine-subtracted part and the background at 5 mg/mL iodine concentration.

Body size	*Slope of contrast media* value							
	0.49	0.50	0.51	0.52	0.53	0.54	0.55	0.56
Small	6.0 (5.4–6.5)	**1.4 (0.9–2.0)**	3.2 (2.6–3.7) p = 0.006	7.8 (7.2–8.3)	12.1 (11.6–12.6)	16.4 (15.9–16.9)	20.7 (20.2–21.2)	26.0 (25.4–26.6)
Medium	5.4 (4.4–6.3)	2.2 (1.0–3.5) p = 0.643	**1.8 (0.9–2.8)**	5.3 (4.2–6.4)	9.1 (7.9–10.2)	13.6 (12.3–14.9)	19.1 (17.5–20.7)	26.5 (24.6–28.3)
Large	8.0 (6.1–9.9)	4.7 (2.8–6.7)	**2.6 (1.4–3.8)**	2.8 (1.2–4.5) p = 0.824	6.0 (3.4–8.6)	10.7 (7.70–13.7)	16.4 (12.8–20.1)	23.6 (19.2–27.9)

Data are shown as mean value (Hounsfield units) and 95% confidence interval (lower–upper). Numbers in bold are the values at the optimal *slope of contrast media* value for each body size. One optimal and one feasible value were obtained for each body size (the *slopes of the contrast media* were 0.50 and 0.51 for the small and medium body sizes and 0.51 and 0.52 for the large body size) and a paired t-test was applied.

body size is slight, the accuracy of iodine subtraction can be expected to be improved by adjusting the SCM value according to the subject's body size when performing iodine dose subtraction.

The optimal SCM value depends on the iodine concentration to be subtracted, and it should be set larger when the iodine concentration is low. It is therefore necessary to adjust the SCM value depending on the scan phase when iodine subtraction is performed; in addition, the quantitative value of iodine will be a benchmark. The default setting of the SCM value for VNC reconstruction in the DECT scanner used in this study is 0.51. Based on our present findings, only an iodine concentration of 10 mg/mL can be subtracted with high accuracy. This is approximately the

Table 5
Difference in the CT number between the iodine-subtracted part and the background at 2 mg/mL iodine concentration.

Body size	*Slope of contrast media* value							
	0.49	0.50	0.51	0.52	0.53	0.54	0.55	0.56
Small	6.2 (5.6–6.8)	4.1 (3.5–4.7) $p < 0.001$	2.2 (1.5–2.8) $p = 0.008$	**0.7 (0.3–1.0)**	2.3 (1.6–2.9) $p = 0.002$	4.6 (3.9–5.2)	6.9 (6.2–7.5)	9.2 (8.6–9.9)
Medium	7.2 (6.6–7.9)	5.6 (4.9–6.3)	4.1 (3.4–4.8) $p < 0.001$	2.5 (1.8–3.2) $p < 0.001$	**0.9 (0.2–1.6)**	1.0 (0.5–1.5) $p = 0.999$	2.3 (1.6–3.0) $p = 0.334$	4.0 (3.2–4.7) $p = 0.010$
Large	8.2 (6.8–9.5)	6.7 (5.4–8.1)	5.5 (4.1–6.8)	4.2 (2.8–5.6)	2.7 (1.3–4.2) $p = 0.339$	1.9 (0.8–3.0) $p = 0.749$	**1.4 (0.3–2.6)**	2.5 (1.4–3.6) $p = 0.087$

Data are shown as mean value (Hounsfield units) and 95% confidence interval (lower–upper). Numbers in bold are the values at the optimal *slope of contrast media* value for each body size. One optimal and more than three feasible values were obtained for the three body sizes and multiple comparison was applied.

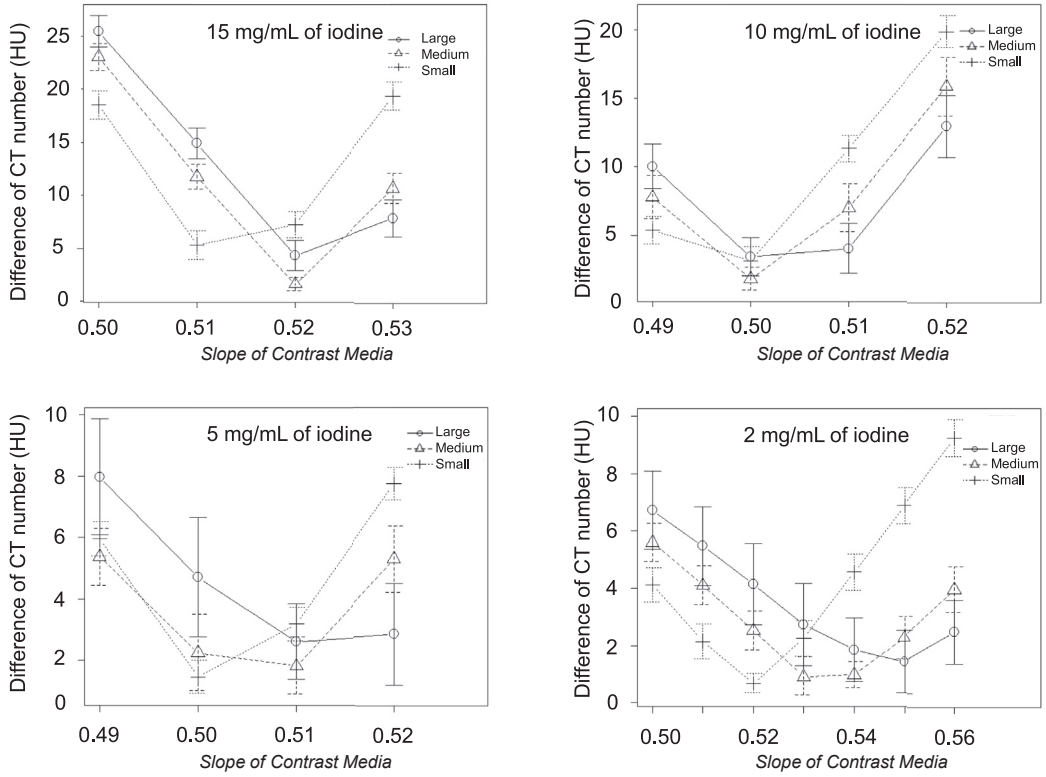

Figure 3. The absolute difference of CT number for each body size at each iodine concentration in the virtual non-contrast image. For all iodine concentrations, the SCM value that achieved the smallest absolute difference of CT number with 95% CIs of <5.0 HU tended to become larger as the body size increased.

appropriate setting for the iodine subtraction of a portal vein in the portal venous phase.[21] Since the degree of contrast enhancement is not the same for all organs, it is possible to improve the accuracy of VNC by limiting the organs to be observed by iodine subtraction (in some cases, only the targeted tumor area) and by using the optimal SCM value. The difference in CT number between TNC and VNC has been reported to exceed 10 HU in 10%–30% of cases due to differences in the scan phase and organs.[9,11,15] The possibility of VNC replacing TNC may be solved by adapting the SCM value used to the iodine concentration of the target organ or site.

Our study revealed that at low iodine concentrations (5 and 2 mg/mL), the SCM value with the smallest absolute differences (95% CI) in CT number was greater at the larger body size. However, the effect of body size was smaller than that of the iodine concentration and was pronounced only at low iodine concentrations. When the iodine concentration was low (2 mg/mL), the degree of iodine subtraction due to the difference in the SCM value of 0.01 was small. Especially in the case of larger body size, there were multiple SCM values that satisfied the CT number difference <5 HU and 95% CI < 5 HU, with the result that only a specific SCM value could not be considered optimal. Therefore, minimum differences in the CT number can be achieved by further adjusting the SCM value according to the subject's body size. In the case of a high iodine concentration (15 mg/mL), the degree of iodine subtraction due to a difference in the SCM value of 0.01 is large, and it is difficult to perform iodine subtraction with an accuracy of <5.0 HU. The generated VNC images show slightly inhomogeneous iodine subtraction at high iodine concentrations. It may thus be difficult to generate accurate VNC images in areas of higher contrast enhancement (e.g., the subclavian artery immediately after contrast administration, or the ureter in equilibrium phase).

We observed that the ratio of the CT number varied with the iodine concentration and was in general agreement with the trend of the optimal SCM value obtained in practice, but the ratio of the

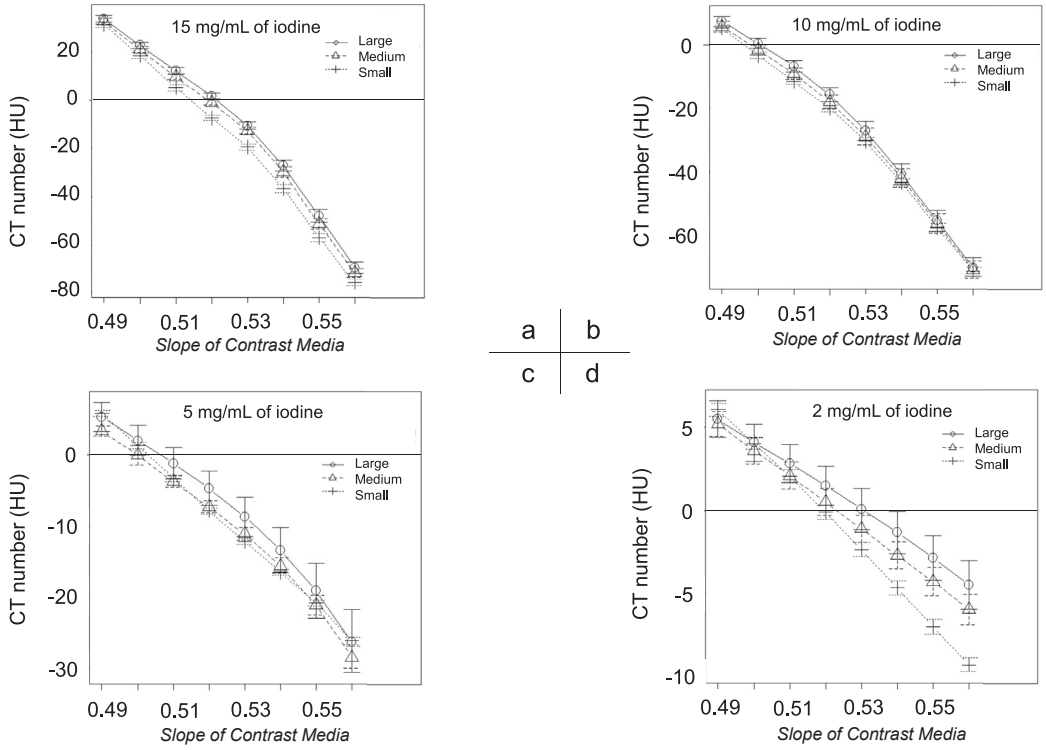

Figure 4. The CT number at each iodine concentration rod in virtual non-contrast images with varying SCM values. The line chart shows the mean and 95% CI values (I bar) of the CT number. At all iodine concentrations, the SCM value at which the CT number approached zero increased with the increase in body size.

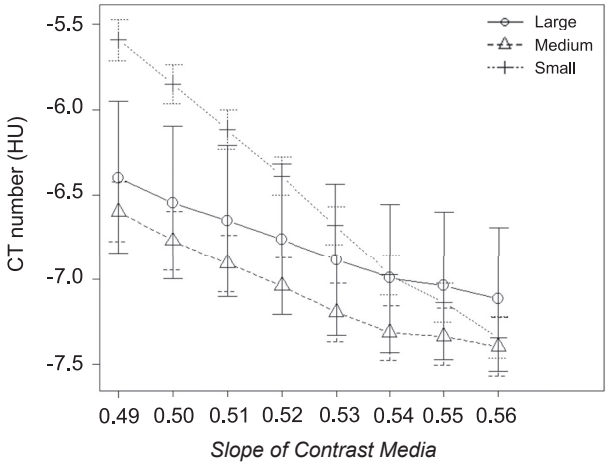

Figure 5. The CT number of the solid water rod in virtual non-contrast images with varying SCM values. The line chart shows the mean and 95% CI values (I bar) of the CT number difference. The differences in the CT number of the solid water increased with the increase in the SCM value.

CT number themselves were different from the actual SCM values. One of the reasons for this discrepancy may be due to the slight subtraction of the attenuation of the solid water, which is without iodine. In the DE process with this CT system, two basis material images (a water image and an iodine image) are first reconstructed and then the virtual monochromatic images followed by VNC images are generated from these two basis material images. The accuracy of these two basis material images thus influences the accuracy of the subsequent DE process. We considered that beam-hardening effects would influence the accuracy of these basis material images. For the range of SCM values considered in this study, the CT number of the solid water part of the VNC images were below 0 HU despite machine calibration. Furthermore, the CT number of the solid water part was slightly subtracted from the attenuation when the SCM value was increased, which suggests that the difference between the iodine part and the solid water part of the VNC image changed, resulting in the difference between the optimal SCM value and the ratio of the CT number. Since the accuracy of the basis material image cannot be adjusted by the user, we believe that the SCM value can be adjusted using these results to improve the accuracy of iodine subtraction.

Here, we propose a method to put the obtained results into practice. As mentioned above, the basis material images of iodine, which are reconstructed first, can be used to measure the iodine concentration in the ROI. This value can be used to assume the approximate SCM value that should be set. To adjust the SCM value further, we can estimate the body size by using the water-equivalent elliptical area displayed on the CT system, which is automatically calculated from the automatic exposure control system. We expect that the combination of these two methods will provide the optimal SCM for material decomposition.

Several limitations of this study should be acknowledged. We did not evaluate clinical images for individual abdominal dynamic DECT. Rather, we focused on the quantitative evaluation of the behavior of the DE process under different iodine concentration conditions and assuming various body sizes. Further studies of the diagnostic performance in clinical settings are needed. In addition, not all possible iodine concentrations and body size combinations were considered in this study, and only the available phantom

conditions were applied. Finally, regarding the DE acquisition and post-processing algorithms released by other vendors, these may differ from the CT system used here, and thus it may be difficult to generalize the present results to the systems of other vendors.

Conclusions

We investigated the optimal SCM value for generating VNC images and evaluated the effects of the iodine concentration and body size by using a phantom. Compared to conventional TNC images, the VNC images obtained by adjusting the SCM value according to the iodine concentration and the subject's body size were more accurate.

Conflict of interest statement

The authors have no conflict of interest to declare.

Acknowledgements

This research did not receive any specific grant from funding agencies in the public, commercial, or not-for-profit sectors.

References

1. Itani M, Bresnahan BW, Rice K, Gunn ML, Wang SS, Revels JW, et al. Clinical and payer-based analysis of value of dual-energy computed tomography for workup of incidental abdominal findings. *J Comput Assist Tomogr* 2019;**43**:605–11. https://doi.org/10.1097/RCT.0000000000000886.
2. Atwi NE, Sabottke CF, Pitre DM, Smith DL, Danrad R, Dharaiya E, et al. Follow-up recommendation rates associated with spectral detector dual-energy CT of the abdomen and pelvis: a retrospective comparison to single-energy CT. *J Am Coll Radiol* 2020;**17**:940–50. https://doi.org/10.1016/j.jacr.2019.12.029.
3. Parakh A, Lennartz S, An C, Rajiah P, Yeh BM, Simeone FJ, et al. Dual-energy CT images: pearls and pitfalls. *Radiographics* 2021;**41**:98–119. https://doi.org/10.1148/rg.2021200102.
4. Graser A, Johnson TR, Hecht EM, Becker CR, Leidecker C, Staehler M, et al. Dual-energy CT in patients suspected of having renal masses: can virtual nonenhanced images replace true nonenhanced images? *Radiology* 2009;**252**:433–40. https://doi.org/10.1148/radiol.2522080557.
5. Zhang LJ, Peng J, Wu SY, Wang ZJ, Wu XS, Zhou CS, et al. Liver virtual non-enhanced CT with dual-source, dual-energy CT: a preliminary study. *Eur Radiol* 2010;**20**:2257–64. https://doi.org/10.1007/s00330-010-1778-7.
6. Toepker M, Moritz T, Krauss B, Weber M, Euller G, Mang T, et al. Virtual non-contrast in second-generation, dual-energy computed tomography: reliability of attenuation values. *Eur J Radiol* 2012;**81**:e398–405. https://doi.org/10.1016/j.ejrad.2011.12.011.
7. De Cecco CN, Muscogiuri G, Schoepf UJ, Caruso D, Wichmann JL, Cannao PM, et al. Virtual unenhanced imaging of the liver with third-generation dual-source dual-energy CT and advanced modeled iterative reconstruction. *Eur J Radiol* 2016;**85**:1257–64. https://doi.org/10.1016/j.ejrad.2016.04.012.
8. Sahni VA, Shinagare AB, Silverman SG. Virtual unenhanced CT images acquired from dual-energy CT urography: accuracy of attenuation values and variation with contrast material phase. *Clin Radiol* 2013;**68**:264–71. https://doi.org/10.1016/j.crad.2012.08.004.
9. Ananthakrishnan L, Rajiah P, Ahn R, Rassouli N, Xi Y, Soesbe TC, et al. Spectral detector CT-derived virtual non-contrast images: comparison of attenuation values with unenhanced CT. *Abdom Radiol* 2017;**42**:702–9. https://doi.org/10.1007/s00261-016-1036-9.
10. Jamali S, Michoux N, Coche E, Dragean CA. Virtual unenhanced phase with spectral dual-energy CT: is it an alternative to conventional true unenhanced phase for abdominal tissues? *Diagn Interv Imaging* 2019;**100**:503–11. https://doi.org/10.1016/j.diii.2019.04.007.
11. Camlidag I. Compatibility of true and virtual unenhanced attenuation in rapid kV-switching dual energy CT. *Diagn Interv Radiol* 2020;**26**:95–100. https://doi.org/10.5152/dir.2019.19345.
12. Botsikas D, Triponez F, Boudabbous S, Hansen C, Becker CD, Montet X. Incidental adrenal lesions detected on enhanced abdominal dual-energy CT: can the diagnostic workup be shortened by the implementation of virtual unenhanced images? *Eur J Radiol* 2014;**83**:1746–51. https://doi.org/10.1016/j.ejrad.2014.06.017.
13. Durieux P, Gevenois PA, Muylem AV, Howarth N, Keyzer C. Abdominal attenuation values on virtual and true unenhanced images obtained with third-generation dual-source dual-energy CT. *AJR Am J Roentgenol* 2018;**210**:1042–58. https://doi.org/10.2214/AJR.17.18248.
14. Kaufmann S, Sauter A, Spira D, Gatidis S, Ketelsen D, Heuschmid M, et al. Tin-filter enhanced dual-energy-CT: image quality and accuracy of CT numbers in virtual noncontrast imaging. *Acad Radiol* 2013;**20**:596–603. https://doi.org/10.1016/j.acra.2013.01.010.
15. Borhani AA, Kulzer M, Iranpour N, Ghodadra A, Sparrow M, Furlan A, et al. Comparison of true unenhanced and virtual unenhanced (VUE) attenuation values in abdominopelvic single-source rapid kilovoltage-switching spectral CT. *Abdom Radiol* 2017;**42**:710–7. https://doi.org/10.1007/s00261-016-0991-5.
16. Miller CM, Gupta RT, Paulson EK, Neville AM, Bashir MR, Merkle EM, et al. Effect of organ enhancement and habitus on estimation of unenhanced attenuation at contrast-enhanced dual-energy MDCT: concepts for individualized and organ-specific spectral iodine subtraction strategies. *AJR Am J Roentgenol* 2011;**196**:W558–64. https://doi.org/10.2214/AJR.10.4858.
17. Kojima T, Shirasaka T, Kondo M, Kato T, Nishie A, Ishigami K, et al. A novel fast kilovoltage switching dual-energy CT with deep learning: accuracy of CT number on virtual monochromatic imaging and iodine quantification. *Phys Med* 2021;**81**:253–61. https://doi.org/10.1016/j.ejmp.2020.12.018.
18. Kanatani R, Shirasaka T, Kojima T, Kato T, Kawakubo M. Influence of beam hardening in dual-energy CT imaging: phantom study for iodine mapping, virtual monoenergetic imaging, and virtual non-contrast imaging. *Eur Radiol Exp* 2021;**5**:18. https://doi.org/10.1186/s41747-021-00217-1.
19. Lambert JW, FitzGerald PF, Edic PM, Sun Y, Bonitatibus Jr PJ, Colborn RE, et al. The effect of patient diameter on the dual-energy ratio of selected contrast-producing elements. *J Comput Assist Tomogr* 2017;**41**:505–10. https://doi.org/10.1097/RCT.0000000000000557.
20. R Core Team. *R: a language and environment for statistical computing*. Vienna, Austria: R Foundation for Statistical Computing; 2021. URL, https://www.R-project.org/.
21. Noda Y, Goshima S, Nakashima Y, Miyoshi T, Kawai N, Kambadakone A, et al. Iodine dose optimization in portal venous phase virtual monochromatic images of the abdomen: prospective study on rapid kVp switching dual energy CT. *Eur J Radiol* 2020;**122**:108746. https://doi.org/10.1016/j.ejrad.2019.108746.